Nanoscale

Accepted Manuscript

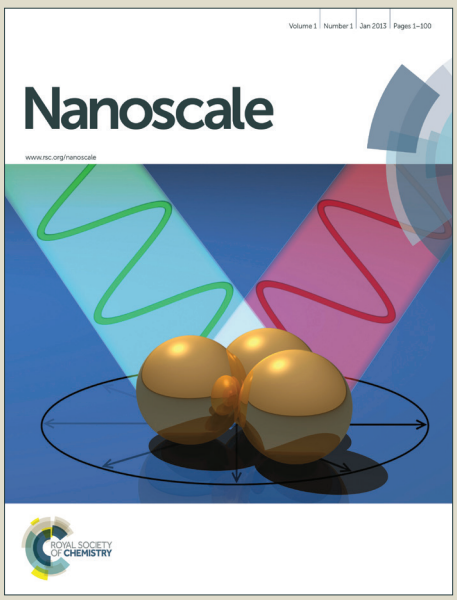

ROYAL SOCIETY OF CHEMISTRY

www.rsc.org/nanoscale

Single-molecule Detection and Radiation Control in Solutions at High Concentrations via a Heterogeneous Optical Slot Antenna†

Chenglong Zhao[a], *Yongmin Liu*[c,d], *Jing Yang*[a], and *Jiasen Zhang*[*a,b]

[a]*State Key Laboratory for Mesoscopic Physics and Department of Physics, Peking University, Beijing, 100871, China.*

[b]*Collaborative Innovation Center of Quantum Matter, Beijing 100871, China. Email: jszhang@pku.edu.cn;*

[c]*Department of Mechanical and Industrial Engineering, Northeastern University, Boston, MA 02115 USA*

[d]*Department of Electrical and Computer Engineering, Northeastern University, Boston, MA 02115 USA*

†Electronic supplementary information (ESI) available. See DOI: xxxxxxxxxxx

We designed a heterogeneous optical slot antenna (OSA) that is capable of detecting single molecule in solutions at high concentrations, where most biological processes occur. The heterogeneous OSA consists of a rectangular nanoslot fabricated on heterogeneous metallic films formed by sequential deposition of gold and aluminum on a glass substrate. The rectangular nanoslot gives rise to large field and fluorescence enhancement for single molecules. The near-field intensity inside a heterogeneous OSA is 170 times larger than that inside an aluminum zero-mode waveguide (ZMW), and the fluorescence emission rate of a molecule inside the heterogeneous OSA is about 70 times higher than that of the molecule in free space. Our proposed heterogeneous optical antenna enables excellent balance between performance and cost. The design takes into account the practical experimental conditions so that the parameters chosen in the simulation are well within the reach of current nano-fabrication technologies. Our results can be used as a direct guidance for designing high-performance, low-cost plasmonic nanodevices for the study of bio-molecule and enzyme dynamics at the single-molecule level.

Introduction

The detection of single-molecule fluorescence[1–5] is a key technique for numerous applications in biomedicines including DNA sequencing,[6,7] diagnostics,[8] and molecular biology.[9] Unfortunately, the detection volume is limited to femtolitre (10^{-15}) in conventional diffraction-limited optics. In addition, the concentration of molecules has to be limited to pico- or nano-molar, so that on average only one molecule is excited inside the diffraction-limited optical spot. This concentration level is far below the micromolar range where many biologically relevant processes occur. Such a limitation can be overcome by using the so-called zero-mode waveguide[10–12] (ZMW), which consists of nanoscale circular-holes milled in an aluminum(Al) film. The key design principle of ZMW is that the light field is mainly confined at the bottom of the nanoholes, acting as small reaction chambers with single molecules inside. The metal film blocks the illuminating light so that only the molecule located at bottom of the nanoholes can be excited and detected while leaving other molecules unaffected. The ZMW allows reduction of the observation volume by 3 to 6 orders of magnitude, from 10^{-15} (with a standard confocal microscope) to 10^{-18} - 10^{-21} liter, allowing for single-molecule detection. ZMWs with different shapes, such as circle,[13,14] rectangle,[15] bowtie,[16] and C-shape[17] have been designed for single-molecule studies. These ZMW structures are commonly fabricated on Al film with light field well confined at bottom but with less field enhancement at visible spectrum compared with that using silver (Ag) or gold (Au). The poor performance for field enhancement further limits the fluorescence emission of a molecule inside these structures according to the optical reciprocity.

Optical nanoantennas, which enable efficient conversion between free space optical radiation and highly localized energy,[18] have attracted extensive attention in recent years for fluorescence enhancement.[19–26] Optical antennas consisting of nanoapertures fabricated on Ag or Au films[27–35] are especially attractive for applications in single-molecule detection at high concentrations. Both the fluorescence emission rate and its radiation pattern can be well controlled using optical antennas due to their strong plasmonic resonances.[36–38] Au is preferable in these applications because of its unique properties such as high

resistance to oxidation and a wide range of available self-assembly molecules.[39–41] In these nanostructures, the light fields at top surface (water-gold) and bottom surface (substrate-gold) tend to be both enhanced because of the strong plasmonic coupling. However, the field enhancement on top is detrimental for detection of single molecules in solutions at high concentrations, because molecules on top surface will also be excited and detected, resulting in increased background noises. It is important to confine and enhance the light field just at the bottom surface so that only molecules in this region can be excited and detected. An optimized design for optical antennas capable of single-molecule detection at high concentrations should satisfy the following requirements: (1) excellent field confinement at bottom; (2) large field and fluorescence enhancement; (3) less field enhancement on top; and (4) excellent balance between performance and cost.

In this paper, we conceptually propose and numerically demonstrate a novel heterogeneous optical slot antenna (OSA) that can fulfill the aforementioned requirements. Compared to ZMWs, the heterogeneous OSAs can substantially enhance the fluorescence of single molecules; while still obtain excellent field confinement and enhancement at the bottom of the antenna. The heterogeneous OSA consists of rectangular nanoslot on a heterogeneous metallic film formed by depositing Au and Al film in sequence on a glass substrate. The numerical simulation shows that the Al film can greatly quench the light field on top of the antenna (water-gold interface) but keep the large field enhancement at bottom (substrate-gold). The field enhancement within a heterogeneous OSA is 170 times larger than that inside a ZMW using aluminum alone. This selective enhancement of optical field at bottom of the antenna makes it especially suitable for enhancing single-molecule detection in solution at high concentrations. Based on this design, we achieved a fluorescence enhancement factor of 70 for single molecules inside the heterogeneous OSA compared to that emitted in free space. The performance and cost of these devices can be well balanced using heterogeneous metallic film. This design principle opens a new avenue for developing high-performance and low-cost plasmonic nanostructures for applications in biomolecule and enzyme dynamics at the single-molecule level.

Numerical Simulation Methods

Finite-difference time-domain (FDTD) method[42] was used for the numerical simulation. The refractive index of water and glass substrate is 1.33 and 1.5, respectively. The optical constants of gold was taken from Johnson & Christy[43] and that of aluminum, titanium and chromium were from Palik.[44] Autonon-uniform meshing with finest mesh size of 1 nm was used for balance between accuracy and computational resources. All the structures in the simulation used the same mesh setting to eliminate the mesh size effects on the final results. Depending on the symmetry of the simulated structures, we applied anti-symmetric or symmetric boundary conditions[42] to further reduce the simulation times, otherwise, perfectly matched layer (PML) boundaries were used. A plane wave with electric amplitude of 1V/m and a wavelength range from 500 to 900 nm was used to illuminate the structure from the glasssubstrate. The polarization of the plane wave was perpendicular to the long axis of the OSA (*x* polarized) as shown in Fig. 1. A molecule was modeled as a classic dipole in the simulation, and the near field was recorded with a power monitor.

Results and discussion

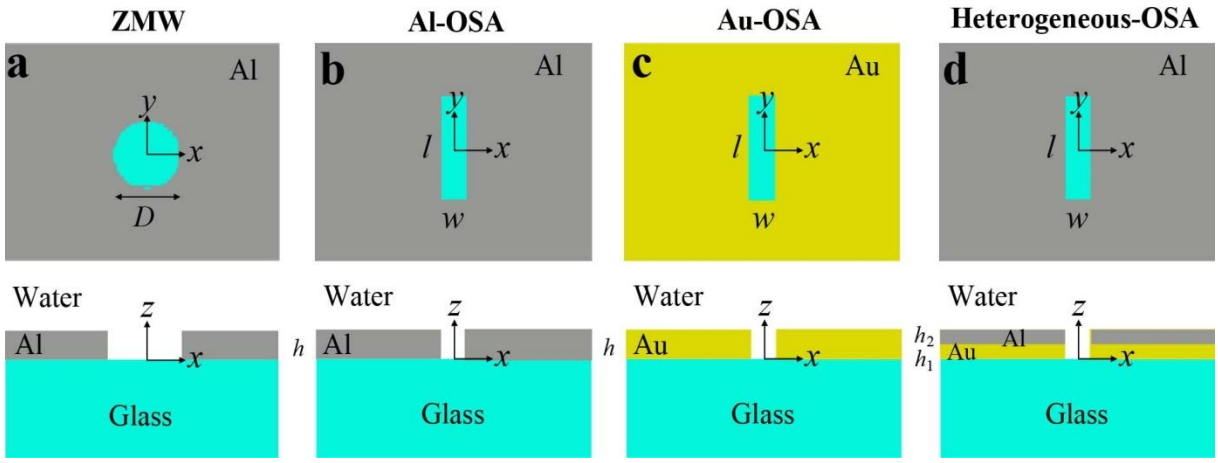

Fig. 1. Schematic of different nanostructures. **a.** ZMW: zero-mode waveguide. **b.** Al-OSA: optical slot antenna on Al film. **c.** Au-OSA: optical slot antenna on gold film. **d.** Heterogeneous-OSA: heterogeneous optical slot antenna. The first row shows the top view of the nanostructures in the *xy* plane. The second row shows the side view of the nanostructures in *xz* plane.

Fig.1a schematically shows a typical ZMW structure that consists of a circular nano-hole milled into 100 nm thick Al film on a glass substrate. In the simulation, the diameter and depth of the ZMW are chosen to be D = 50 and h = 100 nm, respectively, a typical size parameter that was used in most experiments.[12] Fig. 1b shows an optical slot antenna that was etched in Al film (Al-OSA). The Al-OSA consists of a rectangular nanoslot formed in 100 nm thick Al film on a glass substrate. The width, length and depth of the Al-OSA is w = 40, l = 160 and h = 100 nm, respectively. Fig. 1c shows an optical slot antenna that was fabricated on 100 nm Au film (Au-OSA) with parameters w = 40, l = 110 and h = 100 nm, respectively. Fig. 1d shows a heterogeneous optical slot antenna (heterogeneous-OSA) with parameters w = 40, l = 110 and h = 150 nm. The heterogeneous-OSA is made on a heterogeneous film that consists of one layer of 100 nm thick Au film and another layer of 50 nm thick Al film. The three rectangular optical slot antennas shown in Fig. 1b, c and d have better performance than a conventional, circular ZMW as will be discussed below. The designed geometry of OSA is well within the reach of current nano-fabrication technology, such as focused ion beam (FIB) milling. We define the origin (x=0, y=0, z=0) of the system at the bottom center of the nanostructures so that the xy plane at z=0 overlaps with the metal-glass interface. The wavelength dependence of the near-filed intensity is recorded at the origin and all the structures are with water as the superstrate in the following discussions, unless otherwise stated.

The near-field intensity variation as a function of wavelength for the ZMW (red solid curve) was shown in Fig. 2a. The ZMW does not show plasmonic resonance and the near field decreases with increasing wavelength. Fig. 2b shows the near-field distribution of the ZMW in the xz plane at λ = 680 nm. The electric filed is well confined at bottom of the ZMW with negligible fields on top. Such a near-field profile shows exactly how the ZMW works for detecting single molecule at high concentrations. Only molecules that diffuse to the bottom of the nanoholes can be excited and detected while leaving other molecules unaffected. The ZMW shows good field confinement, however, with very weak field enhancement. The black solid curve in Fig. 2a shows the near-field intensity variation as a function of wavelength for an Al-OSA. The Al-OSA shows plasmonic resonance peaked around λ = 680. Its near-

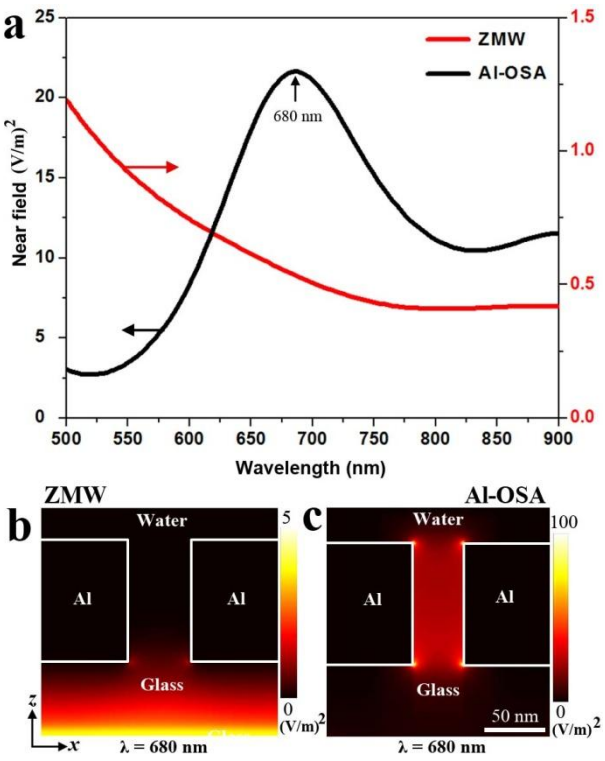

Fig. 2.a. Wavelength dependence of the near-field intensity for a ZMW and an Al-OSA. Near filed was recorded at the origin (x=0, y=0, z=0) of the coordinates as indicated in Fig. 1. **b**. Near-field distribution in the xz plane for the ZMW and Al-OSA at wavelengths λ = 680 nm.

field distribution at λ = 680 nm in the xz plane was shown in Fig. 2c. The near-field intensity at the origin of the Al-OSA is 40 times greater than that of the ZMW at λ =680 nm. The large field enhancement in the Al-OSA will give rise to a higher exciting rate for a single molecule inside the Al-OSA compared to that inside the ZMW. Although the Al-OSA has superior performance regarding to the relative large field enhancements compared to a ZMW, it is well known that Al is not a good plasmonic material in visible wavelengths where most fluorescence biomarkers are excited. Instead, Al has more prominent plasmonic effect in the UV region. Therefore, in the following we investigate an optical slot antenna formed on gold film (Au-OSA) to further optimize the optical fields.

The Au-OSA for better performance was schematically shown in Fig. 1c with parameters w = 40, l = 110 and h = 100 nm. The black solid curve in Fig. 3a shows the wavelength dependence of the near-field

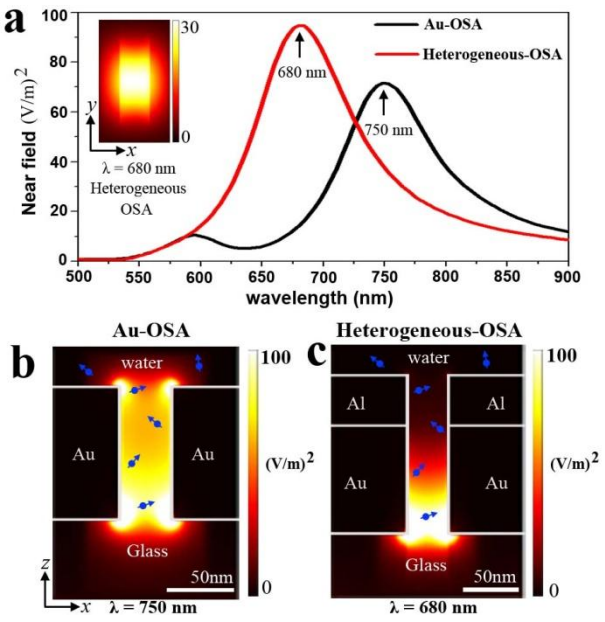

Fig. 3.a. Near-field intensities of the Au-OSA and the heterogeneous OSA versus wavelength. Inset shows the near-field distribution on *xy* plane recorded 20 nm below the lower Au surface (z = -20 nm). **b.** Near-field distribution for the Au-OSA in the *xz* planes at its plasmonic resonant wavelength λ = 750 nm. **c.** Near-field distribution for the heterogeneous OSA in the *xz* plane at its plasmonic resonant wanvelength λ = 680 nm. In **b** and **c**, each molecule is marked as a blue arrow along with a dot.

variation at the origin of the Au-OSA with water as superstrate. The Au-OSA shows two plasmonic resonant peaks (centered at λ =600 and 750 nm) originated from the plasmonic hybridization[45] between the upper (water-Au interface) and lower (glass-Au interface) mode of the Au-OSA. Details about the plasmonic hybridization can be found in the supplementary information Fig. S1 and S2. Fig. 3b shows the near-field distribution of the Au-OSA at the resonant wavelength λ = 750 nm. Clearly, there is a substantial field enhancement at bottom of the Au-OSA with intensity at the origin, 160 times greater than that inside a ZMW. The large field enhancement of the Au-OSA originates from the plasmonic resonance of the slot, which can be easily tuned by changing the size of the slot. The plasmonic resonance of the Au-OSA as a function of its width, length and depth are shown in Fig. S3 in the supplementary information. Briefly, the plasmonic resonant peak redshifts as the length of the slot increases and blueshifts as the width of the slot increases. Decreasing the depth of the slot causes the two plasmonic peaks to separate further apart. Therefore, one can always keep large field enhancement when tuning the OSA's plasmonic

resonance to a desired wavelength. It should be noted that this tenability is hard to achieve with a conventional ZMW. For single molecule detection in solutions at high concentrations, a near-field profile with large field intensity at the bottom while less field intensity at the top of the nanostructure is preferable. Otherwise, the large field intensity on top will also excite molecules and thus increase background noise. Fig. 3b clearly shows that the Au-OSA gives rise to a large field enhancement at bottom as well as on the top. The large field on top is detrimental for detecting single molecule in micro-molar solutions since molecules on the top of the Au-OSA are also excited.

Aimed at getting large field enhancement at bottom while decreasing the field intensity on top, another metal (Al) layer is added on top of the Au-OSA to form a heterogeneous OSA as schematically shown in Fig. 1d. The thickness of the Au and Al film are 100 and 50 nm, respectively. The width and length of the nanoslot is the same with the Au-OSA except that the nanoslot is over etched into the glass substrate to take the practical fabrication into account. The red solid curve in Fig. 3a shows the wavelength dependence of the near-field intensity at the origin for the heterogeneous OSA with water as superstrate. The original two plasmonic peaks (λ = 600 and 750 nm) of the Au-OSA (the black solid curve in Fig. 3a) now degrade into one peak at λ =680 nm after adding the additional Al layer. According to the plasmonic hybridization shown in Fig.S1, the upper (water-Auside) mode is suppressed and only the lower (glass-Au side) mode of the heterogeneous OSA is excited. Notice the plasmonic resonant peak also locates at λ = 680 nm when the thickness of the gold film is 300 nm as shown in Fig. S2. The same plasmonic resonance achieved for these two cases (thicker Au film or Au-Al heterogeneous film) is a direct verification of the mode hybridization. Fig. 3c shows the field distribution of the heterogeneous OSA at resonant wavelength λ = 680 nm. Compared with the field distribution of an Au-OSA shown in Fig. 3b, one can clearly see that the electric field is highly located at the bottom of the heterogeneous OSA. Only the molecule defuses deep into the heterogeneous OSA will be excited leaving other molecules unaffected. In this way, the heterogeneous OSA enables single molecule detection in micro-molar solution just as the

ZMW does but with larger field enhancement. Remarkably, the near-field intensity of the heterogeneous OSA is 170 times larger than that of the ZMW.

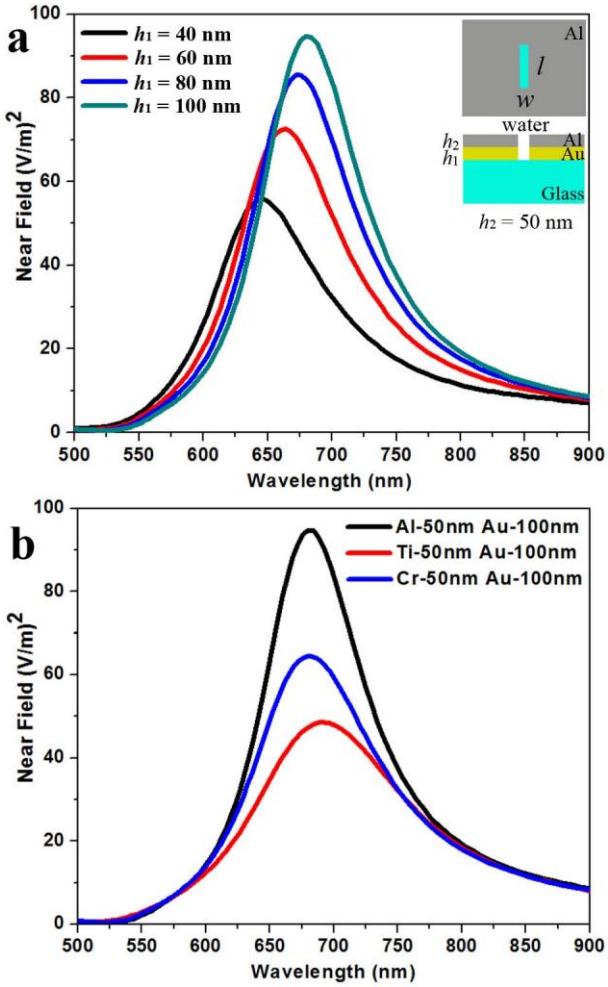

Fig. 4.**a.**Wavelength dependence of the near-field intensity for a heterogeneous OSA with different Au film thickness (h_1 =40, 60, 80, and 100 nm). The thickness of the Al film is kept constant at h_2 = 50nm. Inset schematically shows the structure of the heterogeneous OSA. Near-field intensity was recorded at origin (x=0, y=0, z=0 nm). **b.** Wavelength dependence of the near-field intensity for a heterogeneous OSA with different metal composition: Al-Au, Ti-Au, or Cr-Au. The thickness of the bottom layer (Au) is h_1 =100 nm and the thickness of the top layer (Al, Ti, or Cr) is h_2 =50 nm.

The advantage of using heterogeneous film is two-fold. First, the Au film can greatly enhance the electric field at the bottom of the slot while the Al film can suppress the electric field on top of the slot, which is prerequisite for single molecule detection at high concentrations. Second, it can greatly enhance the

excitation and emission rate of a molecule inside the antenna as will be shown below. In practice, the total thickness of the antenna can be further reduced using either thinner gold or Al film which will be beneficial for fabricating nanoslot with high aspect ratios. Fig. 4a shows the near-field intensity recorded at the origin of the heterogeneous OSA for different gold thickness. The Al film thickness is kept constant at h_2 = 50 nm. The plasmonic resonance blueshifts and the near-field intensity decreases with decreasing gold film thickness. For a heterogeneous OSA with gold and Al thickness of 40 and 50 nm, respectively, the plasmonic resonance blueshifts to λ = 645 nm. The near-field intensity is still 90 times larger than that inside a ZMW. The near-field intensity of the heterogeneous OSA for three different Al thicknesses is shown in Fig. S4a in the supplementary information†. The Au film thickness is kept constant at h_1= 100 nm. The plasmonic resonance redshifts and the near-field intensity decreases with decreasing Al film thickness. Another effect is reducing the Al film thickness increases the field intensity on top of the heterogeneous OSA as shown in Fig. S4b and c, which should be avoided. Therefore, Al film thickness larger than 50 nm is recommended in practical applications. It should be noted that the heterogeneous film is not limited to the combination of Al and gold film. Other non-plasmonic materials such as, titanium (Ti) or chromium (Cr), can also be used. Fig. 4b shows the near-field intensities of three heterogeneous OSAs with Al, Ti or Cr as the top layer. The thickness of the gold film and the top layer is h_1 = 100nm and h_2 = 50 nm, respectively. Fig. 4b shows the near-field intensity as a function of wavelength for the three heterogeneous OSAs. Varying the materials of the top layer has little effects on the plasmonic resonant peak, since the plasmoinc resonance is mainly determined by the gold layer which is kept the same in the three cases. However, the top metallic layer greatly alters the field enhancement inside the heterogeneous OSA. The top layer with an Al film gives the largest field enhancement compared to the case with a Ti or Cr film as the top layer.

The large field enhancement of the heterogeneous OSA will result in a significant fluorescence enhancement for molecules inside the antenna. The fluorescence emission rate γ_{em} is the product of its excitation rate γ_{exc} and quantum yield η. Thus, the fluorescence enhancement can be expressed as:[46]

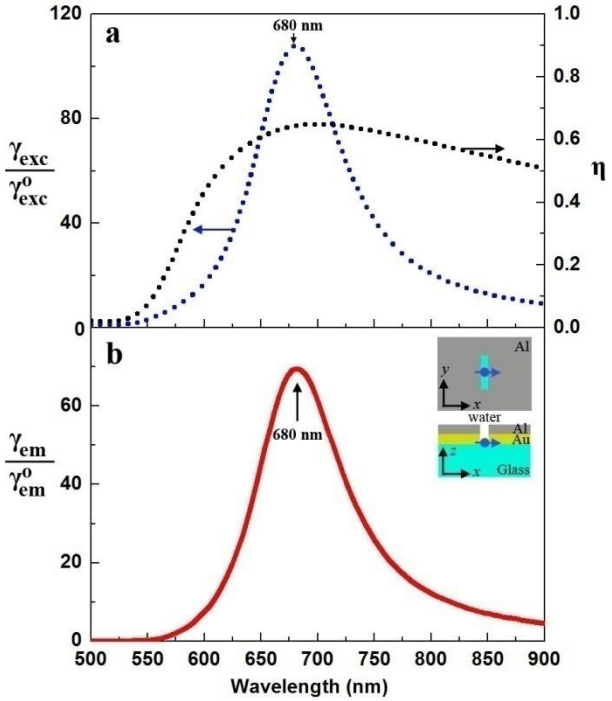

Fig. 5**a**.Wavelength dependence of the normalized excitation rate and quantum yield of a molecule located at *x*=0, *y*=0, *z*=10 nm as shown in Fig. 1c. **b**. Wavelength dependence of the fluorescence enhancement. The inset shows a molecule, represented by a dipole with dipole moment along *x* axis (marked with blue arrow), inside the heterogeneous OSA.

$$\frac{\gamma_{em}}{\gamma_{em}^o} = \frac{\gamma_{exc}}{\gamma_{exc}^o}\frac{\eta}{\eta^o} \tag{1}$$

where the superscript 'o' indicates the corresponding quantity in the absence of the heterogeneous OSA (i.e. free space). The excitation rate is proportional to $|\boldsymbol{p}\cdot\boldsymbol{E}|^2$ if it is not saturated, with $\boldsymbol{p}$ representing the dipole moment and $\boldsymbol{E}$ being the local electric field. η^o is theintrinsic quantum yield in free space and the quantum yield η in presence of the heterogeneous OSA can be expressed as:[46]

$$\eta = \frac{\gamma_r}{\gamma_r + \gamma_{abs} + \gamma_{nr}^o} = \frac{\frac{\gamma_r}{\gamma_r^o}}{\frac{\gamma_r + \gamma_{abs}}{\gamma_r^o} + \frac{1-\eta^o}{\eta^o}} \tag{2}$$

Here, we assume the heterogeneous OSA has negligible influence on the intrinsic non-radiative rate γ_{nr}^o. γ_r and γ_r^o are the radiative decay rate in the presence and absence of the heterogeneous OSA, respectively. γ_{abs} is an additional non-radiative term originated from Ohmic loss in the heterogeneous OSA. The

normalized decay rate are calculated as $\frac{\gamma_r}{\gamma_r^o} = \frac{P_r}{P_r^o}$ and $\frac{\gamma_{abs}}{\gamma_r^o} = \frac{P_{abs}}{P_r^o}$, respectively, with P_r and P_r^o being the power radiated by a dipole in the presence and absence of the heterogeneous OSA, respectively. P_{abs} is the dissipated power within the heterogeneous OSA. We did a spectral analysis of the fluorescence enhancement for a molecule located at *x*=0, *y*=0, *z*=10 nm of the system. For simplicity, we assume the dipole moment of the molecule oriented along the *x* axis so that $p_y = p_z = 0$ and $\eta^o \approx 1$. This is justified since the *x* component of the electric field E_x dominates at this location and only dipoles with *x* component p_x will be effectively excited. In this case, the normalized excitation rate can be simply calculated with the local electric field enhancement as:

$$\frac{\gamma_{exc}}{\gamma_{exc}^o} = \left|\frac{p_x E_x}{p_x E_x^o}\right|^2 = \left|\frac{E_x}{E_x^o}\right|^2 \quad (3)$$

where E_x and E_x^o are the*x* component of the local electric field in the presence and absence of the heterogeneous OSA, respectively. The blue dotted curve in Fig. 5a shows the wavelength dependence of the normalized excitation rate and the black one shows the quantum yield. The molecule obtained an excitation enhancement factor of 108 at λ = 680 nm. The wavelength dependence of the normalized radiative γ_r and nonradiative decay rate γ_{abs} is shown in Fig. S5†. Both γ_r andγ_{abs} are enhanced around the plasmon resonance wavelength. However, γ_r dominates giving rise to a maximum quantum yield η = 0.65 at λ = 700 nm. It is interesting that there is a second nonradiative peak around λ = 550 nm. This peak originated from the longitudinal plasmonic mode of the heterogeneous OSA which can be excited by an incident light with polarization along the long axis of the slot (*y* polarized). The final wavelength dependence of the fluorescence enhancement is shown in Fig. 5b with a maximum enhancement factor of 70 at λ = 680 nm. These results strongly indicate the proposed heterogeneous OSA has superior advantage to enhance the fluorescence emission and reduce the background noise over the conventional ZWM design.

Conclusions

In summary, we have demonstrated with simulation that a heterogeneous OSA, rectangular nanoslot formed on heterogeneous metallic films, has potential applications for enhanced single-molecule detection in solutions at high concentrations where most biological reactions occur. The rectangular structure of the OSA gives rise to strong field enhancement, which results in enhanced excitation and emission rate for single-molecule detections. It should be noted that the performance can be further improved using narrower nanoslot. The heterogeneous films used in the heterogeneous OSA suppress the optical field on top and well confine the field at bottom of the antenna makes single-molecule detection in solutions at high concentrations possible. In practice, the heterogeneous film can be readily prepared using the state-of-the-art depositing technology, which allows depositing multi-layer metals on one substrate in one chamber. The rectangular nanoslot can be readily etched using focused ion beam milling[47], which is a common technique used for fabricating nanoapertures on metallic films. The heterogeneous film is not limited to the combination of gold and Al. One can freely choose other type of metals, such as Ti and Cr, as well. The combination of good plasmonic metals with non-plasmonic metals gives rise to excellent balance between performance and cost. The design principle developed in this paper paves a new way towards high-performance and low-cost plasmonic devices for numerous applications, such as single-molecule detections, DNA sequencing and biomedical diagnosis.

Acknowledgments

This work was supported by the National Natural Science Foundation of China (Grant Nos. 61036005, 61377050, and 11327902) and the Research Fund for the Doctoral Program of Higher Education (Grant No. 20130001110050).

Reference

1. T. Lohmüller, L. Iversen, M. Schmidt, C. Rhodes, H.-L. Tu, W.-C. Lin, and J. T. Groves, *Nano Lett.*, 2012, **12**, 1717–21.

2. Q. Huang, Z. Huang, G. Meng, Y. Fu, and J. R. Lakowicz, *Chem. Commun. (Camb).*, 2013, **49**, 11743–5.

3. A. Singer, S. Rapireddy, D. H. Ly, and A. Meller, *Nano Lett.*, 2012, **12**, 1722–8.

4. V. G. Kravets, F. Schedin, R. Jalil, L. Britnell, R. V Gorbachev, D. Ansell, B. Thackray, K. S. Novoselov, A. K. Geim, A. V Kabashin, and A. N. Grigorenko, *Nat. Mater.*, 2013, **12**, 304–9.

5. P. Zijlstra, P. M. R. Paulo, and M. Orrit, *Nat. Nanotechnol.*, 2012, **7**, 379–82.

6. S. Uemura, C. E. Aitken, J. Korlach, B. A. Flusberg, S. W. Turner, and J. D. Puglisi, *Nature*, 2010, **464**, 1012–7.

7. J. Eid, A. Fehr, J. Gray, K. Luong, J. Lyle, G. Otto, P. Peluso, D. Rank, P. Baybayan, B. Bettman, A. Bibillo, K. Bjornson, B. Chaudhuri, F. Christians, R. Cicero, S. Clark, R. Dalal, A. Dewinter, J. Dixon, M. Foquet, A. Gaertner, P. Hardenbol, C. Heiner, K. Hester, D. Holden, G. Kearns, X. Kong, R. Kuse, Y. Lacroix, S. Lin, P. Lundquist, C. Ma, P. Marks, M. Maxham, D. Murphy, I. Park, T. Pham, M. Phillips, J. Roy, R. Sebra, G. Shen, J. Sorenson, A. Tomaney, K. Travers, M. Trulson, J. Vieceli, J. Wegener, D. Wu, A. Yang, D. Zaccarin, P. Zhao, F. Zhong, J. Korlach, and S. Turner, *Science*, 2009, **323**, 133–8.

8. M. Pitschke, R. Prior, M. Haupt, and D. Riesner, *Nat. Med.*, 1998, **4**, 832–834.

9. K. Bacia, S. A. Kim, and P. Schwille, *Nat. Methods*, 2006, **3**, 83–9.

10. J. M. Moran-Mirabal and H. G. Craighead, *Methods*, 2008, **46**, 11–7.

11. T. Miyake, T. Tanii, H. Sonobe, R. Akahori, N. Shimamoto, T. Ueno, T. Funatsu, and I. Ohdomari, *Anal. Chem.*, 2008, **80**, 6018–22.

12. M. J. Levene, J. Korlach, S. W. Turner, M. Foquet, H. G. Craighead, and W. W. Webb, *Science*, 2003, **299**, 682–6.

13. C. I. Richards, K. Luong, R. Srinivasan, S. W. Turner, D. A. Dougherty, J. Korlach, and H. A. Lester, *Nano Lett.*, 2012, **12**, 3690–4.

14. H. Rigneault, J. Capoulade, J. Dintinger, J. Wenger, N. Bonod, E. Popov, T. Ebbesen, and P.-F. Lenne, *Phys. Rev. Lett.*, 2005, **95**, 117401.

15. J. Wenger, P.-F. Lenne, E. Popov, H. Rigneault, J. Dintinger, and T. W. Ebbesen, *Opt. Express*, 2005, **13**, 7035.

16. G. Lu, W. Li, T. Zhang, S. Yue, J. Liu, L. Hou, Z. Li, and Q. Gong, *ACS Nano*, 2012, **6**, 1438–48.

17. S. Fore, Y. Yuen, L. Hesselink, and T. Huser, *Nano Lett.*, 2007, **7**, 1749–56.

18. P. Bharadwaj, B. Deutsch, and L. Novotny, *Adv. Opt. Photonics*, 2009, **1**, 438.

19. A. Kinkhabwala, Z. Yu, S. Fan, Y. Avlasevich, K. Müllen, and W. E. Moerner, *Nat. Photonics*, 2009, **3**, 654–657.

20. P. Anger, P. Bharadwaj, and L. Novotny, *Phys. Rev. Lett.*, 2006, **96**, 113002.

21. S. Kühn, U. Håkanson, L. Rogobete, and V. Sandoghdar, *Phys. Rev. Lett.*, 2006, **97**, 017402.

22. H. Aouani, S. Itzhakov, D. Gachet, E. Devaux, T. W. Ebbesen, H. Rigneault, D. Oron, and J. Wenger, *ACS Nano*, 2010, **4**, 4571–8.

23. O. L. Muskens, V. Giannini, J. A. Sanchez-Gil, and J. Gómez Rivas, *Nano Lett.*, 2007, **7**, 2871–5.

24. A. G. Curto, G. Volpe, T. H. Taminiau, M. P. Kreuzer, R. Quidant, and N. F. van Hulst, *Science*, 2010, **329**, 930–3.

25. T. H. Taminiau, F. D. Stefani, and N. F. van Hulst, *Opt. Express*, 2008, **16**, 10858.

26. J. N. Farahani, D. W. Pohl, H.-J. Eisler, and B. Hecht, *Phys. Rev. Lett.*, 2005, **95**, 017402.

27. T. Sandén, R. Wyss, C. Santschi, G. Hassaïne, C. Deluz, O. J. F. Martin, S. Wennmalm, and H. Vogel, *Nano Lett.*, 2012, **12**, 370–5.

28. J. T. Choy, B. J. M. Hausmann, T. M. Babinec, I. Bulu, M. Khan, P. Maletinsky, A. Yacoby, and M. Lončar, *Nat. Photonics*, 2011, **5**, 738–743.

29. J. Wenger, D. Gérard, J. Dintinger, O. Mahboub, N. Bonod, E. Popov, T. W. Ebbesen, and H. Rigneault, *Opt. Express*, 2008, **16**, 3008.

30. D. Gérard, J. Wenger, N. Bonod, E. Popov, H. Rigneault, F. Mahdavi, S. Blair, J. Dintinger, and T. Ebbesen, *Phys. Rev. B*, 2008, **77**, 045413.

31. D. Punj, M. Mivelle, S. B. Moparthi, T. S. van Zanten, H. Rigneault, N. F. van Hulst, M. F. García-Parajó, and J. Wenger, *Nat. Nanotechnol.*, 2013, **8**, 512–6.

32. I. Bulu, T. Babinec, B. Hausmann, J. T. Choy, and M. Loncar, *Opt. Express*, 2011, **19**, 5268–76.

33. H. Aouani, O. Mahboub, N. Bonod, E. Devaux, E. Popov, H. Rigneault, T. W. Ebbesen, and J. Wenger, *Nano Lett.*, 2011, **11**, 637–44.

34. Y. C. Jun, K. C. Y. Huang, and M. L. Brongersma, *Nat. Commun.*, 2011, **2**, 283.

35. H. Aouani, O. Mahboub, E. Devaux, H. Rigneault, T. W. Ebbesen, and J. Wenger, *Nano Lett.*, 2011, **11**, 2400–6.

36. T. Ming, L. Zhao, Z. Yang, H. Chen, L. Sun, J. Wang, and C. Yan, *Nano Lett.*, 2009, **9**, 3896–903.

37. T. Ming, H. Chen, R. Jiang, Q. Li, and J. Wang, *J. Phys. Chem. Lett.*, 2012, **3**, 191–202.

38. Y. Fu and J. R. Lakowicz, *J. Phys. Chem. C. Nanomater. Interfaces*, 2010, **114**, 7492–7495.

39. R. G. Nuzzo, B. R. Zegarski, and L. H. Dubois, *J. Am. Chem. Soc.*, 1987, **109**, 733–740.

40. H. Cölfen and S. Mann, *Angew. Chem. Int. Ed. Engl.*, 2003, **42**, 2350–65.

41. A. Doron, E. Katz, and I. Willner, *Langmuir*, 1995, **11**, 1313–1317.

42. *Lumerical FDTD solution*, http://www.lumerical.com.

43. P. B. Johnson and R. W. Christy, *Phys. Rev. B*, 1972, **6**, 4370–4379.

44. E. D. Palik, *Handbook of Optical Constants of Solids II Edited by*, Elsevier Inc., 1997.

45. E. Prodan, C. Radloff, N. J. Halas, and P. Nordlander, *Science*, 2003, **302**, 419–22.

46. P. Bharadwaj and L. Novotny, *Opt. Express*, 2007, **15**, 14266.

47. J. Kim, Y.-G. Roh, S. Cheon, J.-H. Choe, J. Lee, J. Lee, H. Jeong, U. J. Kim, Y. Park, I. Y. Song, Q.-H. Park, S. W. Hwang, K. Kim, and C.-W. Lee, *Nano Lett.*, 2014, DOI: 10.1021/nl500062f.